Coupling between sediment biogeochemistry and phytoplankton development in a temperate freshwater marsh (Charente-Maritime, France): Evidence of temporal pattern

Raphaël Moncelon [a], Marie Gouazé [a], Philippe Pineau [a], Eric Beneteau [b], Martine Bréret [a], Olivier Philippine [c], François-Xavier Robin [c], Christine Dupuy [a], Edouard Metzger [b]

[a] Laboratoire LIENSs, UMR 6250, La Rochelle Université, Bâtiment ILE, 2 Rue Olympe de Gouges, La Rochelle, France

[b] LPG-BIAF, Bio-Indicateurs Actuels et Fossiles, UMR CNRS 6112, Université d'Angers, 2 Boulevard Lavoisier, 49045 Angers Cedex, France

[c] UNIMA, 28 rue Jacques de Vaucanso, ZI de Périgny, 17180 Périgny, France

* Corresponding author: Raphaël Moncelon, LIENSs Laboratory, raphael.moncelon1@univ-lr.fr, +33642306387

Abstract

In freshwater systems, sediment can be an important source for the internal loading of phosphate (PO_4). The limiting character of this element in such system leads to consider this phenomenon in terms of eutrophication risks and water quality stakes. A four-months follow-up (January, March, April and May 2019) was carried out in a strong PO_4 limited secondary channel from an artificial irrigation system of Charente Maritime (France) to link the mobilization of remineralization products in the upper 6 cm layer of sediment (conventional

core slicing/centrifugation and DET probes) and the phytoplankton biomass dynamics in the water column. Results showed congruent patterns between the temporal succession of the organic matter mineralization processes in the sediment and the primary biomass dynamics in the water column. In January and March (considered in winter), PO_4 proved to be retained by adsorption onto iron oxides in anoxic sediment since pore water nitrate inhibited for about a month the respiration of metal oxides in the first cm of sediment, thus limiting PO_4 availability and the phytoplankton growth. In April and May (early spring), after exhaustion of pore water nitrate, the dissolutive reduction of iron oxides released PO_4 into pore water generated a significant diffusive outgoing flux from the sediment to the water column with a maximum in April (-1.10E-04±2.81E-05 nmol cm^{-2} s^{-1}). This release coincided with the nanophytoplankton bloom (5.50 µg Chla L^{-1}) and a potential increase of PO_4 concentration in the water column. This work provides some insight on the importance of benthic-pelagic coupling in anthropogenic systems. This conceptual model has to be deployed on other sites of interest where internal loading of P takes precedence over external inputs and nitrate mitigation drives its benthic recycling and ultimately its bioavailability. This is to be essential to characterize the aquatic environment quality in order to limit eutrophication risks.

Keywords: Freshwater marsh, phytoplankton, early diagenesis, nutrient fluxes, nitrogen, iron, phosphorus

1. Introduction

The importance of wetland ecosystems has been widely recognized for services such as carbon catchment control (Chmura et al., 2003; Sousa et al., 2010) or water purification led by primary producers (Smith, 2003). Phytoplankton structure and dynamics has been well

studied in both marine environments (Legendre and Rassoulzadegan, 1995; Hlaili et al., 2014) and freshwater ecosystems (Tortajada et al., 2011; Masclaux et al., 2014; David et al., 2020a, 2020b). Its development can depend on bottom-up factors such as water temperature, light penetration or nutrient availability (Reid et al., 1990) and/or top-down factors such as grazing or parasitism (Reid et al., 1990; Lynn, 2003), or macrophyte competition (Barrow et al., 2019). The variations of the physical-chemical parameters in the water column and their consequences on phytoplankton dynamics are well documented in marine coastal zones (Justić et al., 1995; Dupuy et al., 2011) and continental freshwater environments (Soballe and Kimmel, 1987; Søndergaard et al., 2017). Temporarily, two blooms are generally mentioned in saline environments, in early spring and late summer (Morais et al., 2003; Toompuu et al., 2003). However, little is known about marsh ecosystems. Research focusing on the variation of water column settings on these dynamics shows a close relation to physical and chemical parameters of the environment both in freshwater or brackish environments. While the phytoplankton dynamics seems to depend less on the season in brackish environments but more on the renewal of water (Tortajada et al., 2011), significant temporal succession has been highlighted in freshwater marshes (Masclaux et al., 2014).

By their position in the watershed, marshes receive huge amounts of nutrients coming from the continent by soil leaching, such as nitrogen (N) and phosphorus (P), essential for primary producers' growth (Redfield, 1958; Søndergaard et al., 2017). Among these elements, P is widely recognized as the principal factor of phytoplankton growth, especially in freshwater systems (Schindler, 1974; Søndergaard et al., 2000; Kraal et al., 2015). Human activities can alter the growth-limiting nutrients, especially through wastewater or various surfaces runoff (Withers and Jarvie, 2008) and can cause eutrophication (Schindler, 1974; Smith, 2003). The reduction of external growth-limiting nutrients as P from shift in management framework would lead to an increase in the importance of sediment as an

internal source (Perkins and Underwood, 2001). In some lowland river systems, P released from organic matter (OM) remineralization in the sediment may even be the main source of P in the water column (van Dael et al., 2020) and thus for the phytoplankton productivity. This loading from sediment could also determinate the P limitation in freshwater ecosystems such as lakes (Wu et al., 2017).

Many techniques exist for calculating diffusive fluxes at the sediment-water interface (SWI), such as the *in situ* use of benthic chambers, or *ex situ* measures through the use of Fick's law (Grenz et al., 1991,Viollier et al., 2003). The latter allow an evaluation of redox processes in the sediment through the modelling of sediment profiles (Grüneberg et al., 2015). More recent techniques such as the use of 2D gel probes provide results (flux and profile modeling) with better vertical and horizontal resolution (Jézéquel et al., 2007; Santner et al., 2015; Thibault de Chanvalon et al., 2017). They make it possible to document the intense gradients that can be expected during P remobilization.

Benthic phosphorus dynamics is well documented, in both marine and freshwater systems (Boström et al., 1988; Caraco et al., 1990; Anschutz et al., 1998; Ekholm and Lehtoranta, 2012), and depends on the evolution of the oxide stocks in the sediment. The iron cycle is of particular interest in understanding the phosphate (PO_4) remobilization, having the capacity of forming relatively stable Fe(OOH)-P complexes preventing its dissolution (Herzsprung et al., 2010). The dynamics of elements interacting with the iron cycle in sediment and influencing its mobilization, such as oxygen, nitrates, manganese, and sulphur, is therefore a major issue in understanding the mechanisms governing the release of PO_4 into the water column (Borggaard et al., 1990; Caraco et al., 1990; Herzsprung et al., 2010; Xiao et al., 2015). Vertical oxidant successions in the first stages of biotic OM mineralization in sediment, called early diagenesis, are well known in marine environments (Froelich et al., 1979; Aller, 2004). However, temporal succession of these processes is poorly documented (Thibault de

Chanvalon et al., 2016). Moreover, retrospective reports on the response of pelagic nutrient and biota are quite frequent (Jeppesen et al., 2005; Welch and Cooke, 2005), but rarely combined with the *in situ* sediment analysis (Grüneberg et al., 2015; Liu et al., 2016).

The high productivity of the Marans' site already observed despite the strong P limitation (Masclaux et al., 2014) testifies to the importance of internal P recycling in this system. The objective of this study is to propose for the first time an interdisciplinary seasonal benthos-pelagos *in situ* monitoring in a strong P-limited coastal freshwater marsh. It is of interest to target such P limited site as environmental policies focuses on limiting P release into natural aquatic systems which consequence is the increase of water bodies characterized by high N/P ratios. The main hypothesis of this work lies on the importance of temporal variation of benthic mineralization processes for the phytoplankton development through generated nutrient fluxes at the SWI. Benthos-pelagos coupling was assessed through a combined ecological and biogeochemical approach, with temporal phytoplankton biomass measurements and nutrient and metal oxides profiling. Diffusive fluxes were obtained from porewater chemical gradients from core slicing (0.5 cm resolution) and 2D-DET gel deployment (submillimeter resolution).

2. Material and methods

2.1. Study site

The Charente Maritime marshes (French Atlantic west coast) present a high diversity of freshwater marsh types, differing by their locality, their role and the way they are managed. A eutrophic freshwater marsh, based on Tortajada classification (2011), used for anthropogenic activities (*e.g.* field irrigation) was chosen to carry out this work. Among the artificial hydrographic networks, the study site took place in a secondary channel of the Sèvre Niortaise

River marshes (46.282°, 0.969°) located closed to the commune of Marans (Fig. S1 as supplementary material). The station is surrounded by crops and cattle lands, and the management (*i.e.* replenishment, drainage and dredging) is provided by a trade union association.

2.2. Sampling strategy and parameters studied

The sediment and the water column compartments were sampled simultaneously and monthly from winter to early spring 2019. The sampling campaigns were realized in January (the 30th), March (the 5th), April (the 2nd) and May (the 1st).

2.2.1. Water column

- Abiotic parameters

At each campaign, *in situ* temperature, salinity and oxygen concentration in the water column were measured with multiparametric sensors (VWR). In addition, these three parameters were monitored continuously (one measurement per 15 minutes) between January (the 30th) and May (the 1st) with HOBO U-26 sensor.

- Phytoplankton compartment

A volume of 15 L of surface water was collected for the phytoplankton sampling in the middle of the channel. The Chlorophyll *a* biomass (Chl*a*) was evaluated for three-size classes of phytoplankton: micro-: >20 µm, nano-: 3 to 20 µm and picophytoplankton: <3 µm. Filters,

made in triplicate (20 µm, 3 µm and 0.7 µm), were used to separate the 3 different size fractions by fractional filtration. The biomass of Chl*a* of each size class was determined by fluorimetry according to the Yentsch and Menzel method (1963).

2.2.2. Sediment compartment

- Core sampling and processing

Four cylindrical cores were collected using PVC tubes (8.2 cm diameter, 20 cm long) with taking care to keep a water thickness of at least 5 cm above the sediment to preserve the sediment-water interface and for bottom water chemistry. Three cores were sliced every 5 mm to a depth of 6 centimetres (i.e. 12 layers) under nitrogen atmosphere. Porewater was extracted from each sediment layer by centrifugation (20 minutes at 2 700g and at *in situ* temperature) then filtered through 0.2 µm filters. Overlying and pore waters were conserved at -20 °C for nutrients analyses, an aliquot was conserved at 5°C for silica analysis in both bottom and pore waters. Aliquots were immediately used for alkalinity measurement and HNO_3 acidification (0.01 mol L^{-1}; Suprapur Merck) for metal analysis. Nutrients *i.e.* nitrates (NO_3^-), nitrites (NO_2^-), soluble reactive phosphorus (SRP), ammonium ($\sum NH_3$) and silica (Si) concentrations were determined by a colorimetric autoanalyser Scalar Seal (whit a detection limit of 0.02 µmol L^{-1}). The acidified aliquot was analyzed by ICP-AES (Thermo Scientific iCAP 6300 Radial) to measure dissolved iron (Fe_d), manganese (Mn_d) and sulphur (S_d). Alkalinity was determined according to the colorimetric Sarazin et al., (1999) method. Absorbance measurements were carried out with a spectrophotomer (SPECTROstar Nano, BMG LABTECH).

The remaining sediment (from centrifugation) was then frozen at -20°C. Samples were freeze-dried and manually grounded for solid phase analyses. Once the samples have been reweighed, the porosity (Ø) was determined for use in fluxes modeling (see next section).

An aliquot (~100 mg) was used for the ascorbate extraction of reactive manganese (Mn^{3+} and Mn^{4+}), iron (amorphous Fe^{3+}) and P according to the method used in Kostka and Luther (1994) and Anschutz et al. (1998).

- High resolution methods

  - *Microprofiling*

A core was placed in an aquarium thermoregulated at the *in situ* temperature and air was injected at the overlying water to maintain O_2 saturation and keep a thin benthic boundary layer. Oxygen was analysed with Clark-type electrodes (50 µm tip diameter, Revsbech, 1989) connected to a Unisense multimeter and a motorized vertical micromanipulator. A two-point calibration was made from saturated overlying water and anoxic sediment.

  - *2D-DET probes*

In April, two supplementary cores were collected for a 2D-DET probes deployment. This method uses a Diffusive Equilibrium in Thin films (DET) probe (Davison et al., 1991), coupled with a colorimetric technique to visualize in two-dimensions the repartition of dissolved nitrite iron and P concentrations along the core (Jézéquel et al., 2007, Pagès et al., 2011, Metzger et al., 2016). Firstly, a DET gel probe which samples the dissolved chemical

species from the pore water at high resolution fixed to a Plexiglas plate was introduced into the sediment core.

This probe was made of a 185 mm×125 mm×0.8 mm polyacrylamide thin film (Krom et al., 1994) laid on an acrylic support and a PVDF porous (0.2 µm) membrane that maintained and protected the gel in order to minimize lateral heterogeneity. For a single support, 2 gels were placed back to back to make a double-faced probe. The first probe had a gel dedicated to nitrite and another to iron, the second had a probe dedicated to P, the other to iron. After 5-hours equilibrium time, gel probes were quickly processed to minimize lateral diffusion within the sampling gel and subsequent loss of 2D resolution. It consisted in superimposing each gel into a specific reagent gel previously equilibrated with NO_2, PO_4 and Fe colorimetric reagents (Griess, molybdate, ferrozine reagents, see references cited above). Twenty minutes after contact, a picture was taken with a standard scanner. Images were analyzed by densitometry of different RGB spectral bandwidths using ImageJ software. The iron was treated in the blue channel. This channel was chosen despite its lower sensibility compared to the green one in order to avoid saturation (range between 0 and 500 µmol L^{-1} for the blue channel, between 0 and 200 µmol L^{-1} for the green one). Phosphates and nitrites were analyzed in the red and green channel respectively.

- Diffusive fluxes modeling

NO_3^-, NO_2^-, ΣNH_3, SRP, Si, Fe_d and oxygen (O_2) diffusive fluxes at the SWI were determined using the Profile software (Berg et al. 1998). Based on a transport-reaction model, this software allowed to describe the sedimentary column as a succession of layers with a specific reaction rate for a dissolved chemical species and the fluxes above and below that sediment column (modeling vertical domain). This work focused on the vertical diffusion and

the transport was assumed to be dominated by molecular diffusion (without bioturbation), as described in Lewandowski et al., (2002), since the sediment is impermeable (silt-clay). The flux (F) was calculated at the SWI thanks the Fick Law as:

$$(1)\ F = -\phi Ds(dC/dz)$$

with ∅ the sediment porosity, *Ds* the diffusion coefficient, *C* the element concentration and *z* the depth of calculation. In Profile, Ds was calculated using Rasmussen and Jorgensen (1992), as below:

$$(2)\ Ds = D/(1+3(1-\emptyset))$$

Diffusion coefficient *D* was determined with previous studies varying with temperature. O_2 fluxes modeling were made using data from microprofiling, *D* was taken from the Unisense gas table. The NO_3^-, NO_2^-, ΣNH_3 and SRP coefficient diffusion were taken from Li and Gregory (1974), and the Si one from Rebreanu et al. (2008). Modeling was based on data from the core slicing and 2D-DET profiles. In case of too few points with quantified concentrations a linear model was used to calculate the flux "manually" (Boudreau, 1997) using the formula (1) and Ds as :

$$(3)\ Ds = D/(1-\ln(\Phi^2))$$

In this work, the negative flux values corresponded to fluxes leaving the sediment, the positive values to fluxes entering the sediment. O_2, NO_3^-, ΣNH_3 and Si fluxes were calculated through profiles obtained with the core slicing method. NO_2^-, SRP and Fe fluxes were calculated through both core slicing method profiles and 2D-DET probes. The fluxes calculated from the 2D-DET probes represented the width-integrated average fluxes of the gel at three interfaces positioning: 0 (SWI), SWI+1 mm and SWI-1mm. The flux was modeled from the mean concentrations per gel line. The overlying water was not used for the

calculation of the gradients at the interface, because of the very strong chemical gradients near the diffusive boundary layer (DBL) and not reflecting its chemical properties.

2.3. Statistical tests

All statistical tests were made with the software R studio (1.2.1335). Analyses of Variance (ANOVA) and Tuckey post hoc tests (threshold $\alpha = 0.05$) were made to determinate significant differences between replicates. To respect the validity of this statistical test, data could be log transformed. If residuals did not followed normality, Kruskal Wallis and Wilcoxon post-hoc tests were made.

3. Results

3.1. Physical-chemical parameters of the water column

Temperature increased regularly between the end of January and May, rising from 8°C to 15°C on average in the channel (Fig. 1). Discrete sampling points indicated (measured with WTW sensor) 7.5, 10, 14 and 14°C for January, March, April and May respectively. Conductivity was relatively stable around 850 µS cm^{-1}, which represents a salinity around 0.5. Dissolved oxygen increased between late January and late February (approximately 5 to 17 mg L^{-1}). From April to May, it decreased on average from about 17 to 10 mg L^{-1}. Discrete sampling indicated subsequently 9, 11, 14.5 and 11.3 mg L^{-1} for January, March, April and May respectively.

Nitrogen was mainly represented by NO_3^- with the highest concentration (668 µmol L^{-1}) observed in March (Tuckey test, $F(3) = 7.58$, $p < 0.05$) (Table. 1). NO_2^- concentration was the

highest in April (20.43 µmol L^{-1}) (Tuckey test, $F(3) = 14.06$, $p < 0.05$). ΣNH_3 concentration was higher in April (79 µmol L^{-1}) than those of January and March (Kruskal-Wallis test, $\chi^2(3) = 8.66$, $p < 0.05$). SRP increased over time, from 0.00 to 0.37 µmol L^{-1} in March and May respectively. However, no significant differences were noted despite the increase (Kruskal-Wallis test, $\chi^2(3) = 5.64$, $p < 0.05$). Finally, Si concentration in April (154 µmol L^{-1}) was higher than for March (Kruskal-Wallis test, $\chi^2(3) = 3.17$, $p = 0.05$). According to Redfield ratio calculations (Fig. S2 as supplementary material), the study site was only phosphate-limited for planktonic primary producers, all along the survey.

3.2. Phytoplankton dynamics

From January to March, the phytoplankton biomass was between 1 and 3.4 µg Chla L^{-1} depending on the size class, and dominated by the microphytoplankton (Fig. 2). However, no significant difference was observed between the three size classes neither in January (ANOVA, $F(2) = 1.21$, $p > 0.05$) nor in March (ANOVA, $F(2) = 3.55$, $p > 0.05$). In April, a significant nanophytoplankton development was observed with 5.5 µg Chla L^{-1} (Tuckey *post Hoc* test, $p < 0.001$). A similar pattern was observed in May, with a dominant nanophytoplankton biomass, four times higher than that of the other two size classes (4 and 1 µg Chla L^{-1} respectively) (Tuckey *post Hoc* test, $p < 0.001$).

Within each size class, the April nanophytoplankton and picophytoplankton biomasses (5 and 3 µg Chla L^{-1} respectively) were higher than in January, March and May (Tuckey *post Hoc* test, $p < 0.03$ and $p < 0.001$ respectively).

3.3. Sediment geochemistry

In late January, NO_3^- mean concentration was around 200 µmol L^{-1} with high spatial variability between 0 and 2 cm depth and decreased sharply to reach about 5 µmol L^{-1} at 3.5 cm depth (Fig. 3). Same pattern was observed for NO_2^- with a maximum mean concentration in the top layer (43 µmol L^{-1}) which decreased rapidly to reach the detection limit at 3.5 cm depth. Early in March, only the first sediment layer showed detectable nitrate and nitrite with 37 and 6 µmol L^{-1} respectively. Then, no sample showed detectable concentrations.

Mn_{asc} showed a maximum concentration in late January in the first layer of sediment (3.2 mmol kg^{-1}) and remained constant downwards at 1.5 mmol kg^{-1}. For March, April and May, values ranged between 1.0 to 1.5 mmol kg^{-1}. Mn_d presented a linear increase along the core in January, April and May between 1 to 60 µmol kg^{-1}. A peak was observed in March between 0 and 3 cm, with a maximum of 35 µmol kg^{-1}.

Fe_{asc} was higher in January and May around 25 mmol kg^{-1} and lower in March and April around 20 mmol kg^{-1}, until 4 cm depth. In late January, Fe_d was near the detection limit from 0 to 5 cm, and in March a first peak was observed at 1.5 cm (47 µmol kg^{-1}) at the same depth as the manganese one. In April, a strong mobilization was detected between the surface and 4 cm deep with a peak of 152 µmol kg^{-1}. It then increased to 238 µmol kg^{-1} in the deepest layers. In May, at the same depth dissolved iron peaked at 70 µmol kg^{-1}, to then reach 232 µmol kg^{-1} at 6 cm depth. In April and May, Fe_d increased from 4 and 3 cm depth respectively to reach more than 200 µmol L^{-1} at the core bottom.

P_{asc} ranged between 4 and 5 mmol kg^{-1} in January, March and May, without any real trend with depth. It was higher in April to reach between 5 and 6 mmol kg^{-1}. SRP was under detection limit in January. A first peak of 3 µmol L^{-1} appeared at 1.5 cm depth in March (concomitant with manganese and the first iron peak) to increase in April, with a strong mobilization in the first 2 cm with a maximum of 32 µmol L^{-1}. In May, a weaker and deeper peak was observed (3 cm depth, 22 µmol L^{-1}). These two peaks seemed to coincide with the

globally increase of dissolved iron mobilization in the first 4 cm of sediment, especially in April.

Sulphate profiles showed generally increasing concentrations with depth, with the highest concentrations observed in January (2 to 8 mmol kg^{-1} at surface and depth respectively). In March, April and May, concentrations ranged from about 0.5 mmol kg^{-1} at the surface to 3 mmol kg^{-1} at depth. Concentrations in April were the lowest and showed the smallest gradient (between 0.5 and 1.5 mmol kg^{-1}) along the sediment.

For both January and March, ΣNH_3 concentrations ranged from nearly 50 µmol L^{-1} to 130 µmol L^{-1} between top layer and 6 cm deep respectively, with a slight increase in the last centimeter. ΣNH_3 concentrations in April and May were about 4 times higher than those obtained in winter in the surface layer (193 and 175 µmol L^{-1} respectively), and presented a maximum peak in May at 3 cm depth to reach 439 µmol L^{-1}.

Si had the same vertical trend for every month with a slightly increasing concentration along both the core column and time. Maxima observed were at around 5 cm depth, with 411, 496, 583 and 682 µmol L^{-1} for January, March, April and May respectively.

The alkalinity increased over months and was positively correlated with ΣNH_3 concentration in porewater ($p < 0.001$, $r^2 = 0.76$). In January, it ranged between 6.5 and 7.7 mmol kg^{-1} at the surface and core bottom layer respectively, with a slight increase in the last centimeter. It then increased from Marsh (between 7.0 and 8.9 mmol kg^{-1}) to April (between 10.5 and 13.5mmol kg^{-1}).

The 2D representation of dissolved iron, nitrite and SRP in the sediment pore water was made in April (Fig. 4). Both iron gels (probe 1 and 2) showed an increasing concentration with depth (Fig. 4), with mobilization starting at nearly 0.5 cm below the SWI and increased sharply from 15 to 170 µmol L^{-1} at 1.5 cm depth for probe 1 and from 30 to 170 µmol L^{-1} at 2.5 cm depth for probe 2. The concentrations then increased slightly to reach a maximum of

290 µmol L^{-1} and 240 µmol L^{-1} at 12 cm deep for probe 1 and probe 2 respectively. On probe 1, nitrite was only present in a thin layer between the SWI and 1 cm depth (maximum concentrations of about 65 µmol L^{-1}). The average SRP (probe 2) presented a strong mobilization between 1 and 6 cm with a maximum concentration about 90 µmol L^{-1}. The lateral heterogeneity was more pronounced on probe 1(*e.g.* Fe_d-depleted and NO_2-rich zones between 5-9 cm and 0-2 cm depth respectively, on a 2 cm width).

The Fe_{asc}/P_{asc} ratio is an interesting indicator to understand the effects of the adsorption site saturation on the remobilization of P in the porewater (Anschutz et al. 1998, Thibault de Chanvalon et al 2016). Between 1 and 5 cm deep, in January and May Fe_{asc}/P_{asc} ratio was quite similar around 6. (Fig. 5). In March and April, this ratio was lower around 5 and 4 respectively.

3.4. Benthic fluxes and high spatial resolution consideration

Incoming oxygen fluxes were observed (around 10^{-2} nmol cm^{-2} s^{-1}), with maximum fluxes in May significantly higher than those of March (Kruskal-Wallis test, $\chi^2(3) = 12.19$, $p = 0.03$). The nitrogen nutrient fluxes were most heterogeneous, recording ingoing and outgoing fluxes depending on the element studied. Ingoing NO_3^- and NO_2^- fluxes were observed for each date with a significantly higher flux in January (4.53E^{-03} nmol cm^{-2} s^{-1}; Tuckey test, $F(3)= 6.48$, $p<0.05$ and 5.06E^{-04} nmol cm^{-2} s^{-1}; Tuckey test, $F(3) = 5.87$, $p < 0.05$ for NO_3^- and NO_2^- respectively). Lastly, ΣNH_3 fluxes tended to be outgoing for each date. No significant differences were noted between dates (Kruskal-Wallis test, $\chi^2(3) = 4.59$, $p = 0.20$). A slight SRP influx in January and efflux between March and May was observed. The outgoing flux in April (-1.10E^{-04} nmol cm^{-2} s^{-1}) was significantly higher and 10 times greater compared to ones in March (Tuckey test, $F(3) = 12.51$, $p < 0.005$). The Si fluxes showed an

outgoing flux for each date. No significant differences were noted (Tuckey test, $F(3) = 2.06$, $p = 0.18$). Finally, the iron flowed out regardless of the date. The February flux ($-2.10E^{-06}$ nmol cm^{-2} s^{-1}) was significantly lower than those of March, April and May (Tuckey test, $F(3) = 10.38$, $p < 0.05$).

The fluxes calculations via the modeling of 2D gel concentrations showed the impact of the core scale heterogeneity on the fluxes and the importance of interface positioning (Table 3). At the 0 interface, NO_2^- and SRP presented an incoming flux of the order of 10^{-5} and 10^{-6} µmol cm^{-2} s^{-1} respectively. A Fe_d efflux was observed around $-2E^{-04}$ nmol cm^{-2} s^{-1}.

The change in the interface positioning generated variability in flux directions. For NO_2^-, a +/- 1mm positioning generated a mean outgoing (10^{-5} µmol cm^{-2} s^{-1}) and incoming (10^{-4} µmol cm^{-2} s^{-1}) flux respectively. For SRP, these two positions produced an outgoing flux of the same magnitude order (10^{-5} µmol cm^{-2} s^{-1}). Only the averaged iron fluxes were always outgoing whatever the interface considered, which showed a better homogeneity in the upper part of the gel.

4. Discussion

4.1. Phytoplankton dynamics and nutrients availability

The phytoplanktonic dynamics observed at Marans can be qualified as relatively classic for a freshwater system (Tortajada et al., 2011). A poor development in winter regardless of the size classes was explained by the unfavorable physical conditions (low temperature and probably luminosity) despite huge nitrates values in March (Table 1) probably coming from near agricultural soil leaching (Tortajada et al., 2011). The nanophytoplankton bloom

observed in April could be attributed to much more favorable physical conditions (increase in temperature and probably luminosity), but also in nutrient charging of the system, and especially in dissolved phosphorus (see below for link benthos/pelagos coupling) as strong limiting factor (Kraal et al., 2015; Horppila, 2019). These very weak concentrations of SRP, not exceeding 0.4 µmol L^{-1}, were of the same magnitude order as those measured in the work of David et al (2020a) in a comparable environment. Such weak concentration could suggest a constant upstream to downstream flow of water preventing its accumulation or a rapid withdrawal by autotrophic organisms (Masclaux et al., 2014).

The P limitation at Marans could induce competition between different phytoplanktonic communities. The high surface area/volume ratio and the active metabolism of nanophytoplankton and picophytoplankton make them more efficient to uptake nutrients than larger cells (microphytoplankton) (Legendre et Rasoulzadegan 1995; Masclaux et al., 2014) which could explain the dominance of nanophytoplankton at early spring in this study.

However, these dynamics over time was not entirely consistent to those observed in comparable systems. If a slight spring development of nano-microphytoplankton was observed in David et al. (2020a), the real difference appeared to occur in March, when a strong microphytoplankton development has been observed in other works, in addition to the pico-nanophytoplankton (Masclaux et al., 2014). The absence of such a development in this work would suggest that a possible bloom took place between sampling dates, in line with the potential fast phytoplankton response to environmental changes (Thyssen et al., 2008). Indeed, the decrease of nitrate in the water column from March to May (668 to 371 µmol L^{-1}) as well as the increase of the dissolved O_2 concentration (Fig 1) could indicate a nutrient uptake by primary producers as observed in April that would have started before (Masclaux et al., 2014). Moreover, P limitation in Marans did not allow a strong development with regard

to the Redfield ratio (Justić et al., 1995), but shift in such limitation could be possible, attributed to the endogenous recycling of P (Wu et al., 2017) through diagenetic processes.

4.2. Temporal succession of dominant diagenetic processes

4.2.1. Initial condition : winter situation

The high NO_3^- concentration in the water column and the high NO_3^--NO_2^- concentration in January between the interface and 3 cm depth suggested water column as the main nitrate source for the sediment, rather than nitrification in the sediment of low-nitrate environments (Middelburg et al., 1996). The strong NO_3^--NO_2^- gradient in these sediment layers (Fig. 3) led to consider denitrification as the main process for nitrogen removal since the only slight reduction to ammonia (DNRA) occur in the sediment (Binnerup et al., 1992; Rysgaard et al., 1993)

Here, denitrification appeared to indirectly inhibit the SRP remobilization, by inhibiting the reduction of iron oxides (Wauer et al., 2005; Petzoldt and Uhlmann, 2006; Schauser et al., 2006; Grüneberg et al., 2015) whereas Mn and Fe cycles quickly dominated early diagenetic processes in coastal marine sediment (Pastor et al., 2018). Indeed, the only trace-state presence of SRP congruent with the non-detection of Fe_d and the relatively large stock of iron oxide along the profile (Fig. 3) suggested a low iron oxide reactivity. The high NO_3^- concentration in the surficial sediment in winter, plus the probable thin oxic layer, could promote iron oxidation and explain the maximum Fe_{asc} values and the Mn_{asc} peak at the sediment surface (Fig. 3) (Hansen et al., 2003; Burgin et al., 2011). These high oxides concentrations allow a great amount of adsorption sites for PO_4, which would be immediately uptaken during OM mineralization. The deeper Fe_{asc} values could be explained by a ferrous

fraction Fe^{2+} associated with iron monosulphide (Kostka and Luther, 1994; Anschutz et al., 1999). The constant increasing gradient of Mn_d could be generated by dissolutive manganese reduction during OM mineralization following the appearance of favourable redox conditions. Another possible source of dissolved manganese could be the reduction of manganese oxides by reduced iron diffusion from a deeper source. Moreover, the concomitant low P_{asc} (Fig. 3) and low SRP values in January could suggest that mineralization was still low at this time of the year. Moreover, in considering ΣNH_3 and alkalinity in porewater as a tracer of anaerobic mineralization processes, their slight increase in the last cm seemed to indicate the occurrence of such processes under the sampling area (Fig. 3).

4.2.2. Spring time evolution

In March, the slight presence of nitrate and nitrite in sediment surface indicated that the denitrification became shallower. Overlying waters were more concentrated (Table 1) probably due to inputs from watershed, suggesting that denitrification was relatively fast, limiting diffusion of nitrate and nitrite downwards. Moreover, the non-accumulation of ΣNH_3 between January and March (Fig. 3) would be consistent with annamox reaction for the nitrogen removal, possible as long as NO_3^- was not totally depleted (Canfield et al., 1993). However weak gradients of ΣNH_3 in the surficial sediment made this hypothesis unlikely. The peak of Mn_d also suggested a consumption of manganese oxides for mineralization of OM in the first 3 cm (Fig. 3) as evidenced by the decrease in Mn_{asc} at the surface between January and March, which could lead to the first remobilization of phosphorus explained by the slight peak of SRP at 1.5 cm depth. The presence of a first Fe dissolved peak concurrent to the dissolved Mn one also suggested the beginning of the consumption of Fe^{3+} hydroxides as a terminal electron acceptor for the degradation of OM. This seemed to be consistent with the

decrease of Fe_{asc} in the sediment at that time. This decrease could also be attributed to the non-efficient Fe^{2+} reoxidation due to the absence of NO_3^- and the thin oxic layer. The quantities of oxides were certainly still too high to permit a significant diffusive P flux into water column (Table 2) as shown by the high ratio Fe_{asc}/P_{asc} (Fig. 5) and the rather weak mineralization.

The total depletion of nitrate and nitrite in the sediment from April (Fig. 3) and the increase in temperature (Fig. 1) were favourable factors for triggering the chemical and microbial reduction of iron hydroxides (Jensen et al., 1995) as OM mineralization pathway. The sharp increase in Fe_d in the porewaters within the first 4 cm in April and the second peak in the first 3 cm in May was an evidence of the iron oxides consumption (Fig. 3). As a result, the phosphate sorbed onto iron hydroxides was released into interstitial waters and seemed to be the main route for SRP mobilization, rather than the dissimilatory sulphate reduction observed in estuarine systems (Pan et al., 2020). The phosphate mobilization attributed to the 4 first cm in spring was the highest and most superficial in April, according to P_{asc} diminution in the first cm (Fig. 3). A significant SRP efflux was observed at that time (Table 2). 2D gels realization in April allowed to validate and strengthen the link between iron and P cycle observed via core slicing profile within the upper part of the sediment in Marans (Fig. 4) (Pan et al., 2019). Moreover, the overall trend of Fe_d to increase in depth, as for Mn_d, suggested more favourable redox conditions for the OM mineralization via the iron reduction route.

The OM mineralization could also be identified via the sharp increase in alkalinity (Sholkovitz, 1973) and mineralization products in sediment porewaters (ΣNH_3, Si) until May (Fig. 3). The maximum concentrations of P_{asc} in April (Fig. 3) could be explained by SRP sorption on the hydroxides during their diffusion throughout the sediment. The minimum Fe_{asc}/P_{asc} ratio (Fig. 5), following the consumption of metal oxides, could indicate a kind of saturation of the Fe adsorption sites with respect to P (Anschutz et al., 1998). The excess in

mobilisation of SRP in the upper part of the sediment could explain the diffusive flux into the water column in April and May (Table 2).

However, an Fe_{asc}/P_{asc} ratio < 2 showed the non-sufficiency of FeOOH to prevent the diffusion of P into the water column in lake systems (Gächter and Müller, 2003). The constant Fe_{asc}/P_{asc} > 3 in this work could suggest the existence of another phase that precipitates with Fe^{3+} such as FeS_x, which could be consistent with the potential sulphate reduction supposed by the decrease of soluble sulphur compounds over time (Fig 3). The increasing of Fe_d in depth in April and May (Figs 3, 4) could be coming from the Fe^{2+} resolubilisation following abiotic reduction between S^{2-} and a Fe^{3+} source or FeS_x dissolution (Johnston et al., 2014) below the iron hydroxide respiration zone.

The increase of Fe_{asc} concentrations in May in the first 3 cm may also suggest a highly crystallised ferric form that would not react with P and thus explain the non-correlation between Fe_{asc} and P_{asc} in this sediment layer. On this assumption, the probable non-saturation of the surface sites of iron oxides by phosphate ions, (high Fe_{asc}/P_{asc} ratio) could allow Fe^{3+} to recrystallize (Anschutz et al., 1998) and explained the slight SRP efflux observed in May (Table 2). Moreover, the more important residence time of dissolved P compared to Fe_d in sediment could explain this Fe_{asc}-P_{asc} phase shifting in May (Millero et al., 1987; Neupane et al., 2014; Giles et al., 2016; Smolders et al., 2017; Ding et al., 2018) and favor P mobilization (Thibault de Chanvalon et al., 2016).

The chemical species distribution presented vertical and horizontal heterogeneity at centimeter scale and could make difficult the interpretation of their layering in the sediment column. This heterogeneity could be directly observed through 2D-DET probes, especially concerning iron and nitrite gels (Fig. 4). These distributions can be impaired by macroorganisms burrows or root systems in the sediment which can strongly influence its geochemistry by promoting O_2 and nitrate inputs (Christensen et al., 1997; Frederiksen et

Glud, 2006; Cesbron et al. 2014; Aller et al., 2019) or impacting the vertical and horizontal distribution of solids (Thibault de Chanvalon et al., 2016). Such heterogeneity is also evidenced at the station scale by the variability between core triplicates.

4.3. Sediment and biochemical parameters retroaction of the water column

The flux directions from profiles out of the core slicing method were relatively consistent with the surface gradients observed via mean nutrient profiles in the sediment, indicating a good fit between actual and modelled data. The high-resolution method tends to decrease fluxes by reducing the chemical gradients at the interface (Table 3). The heterogeneity in chemical species distribution (evidenced on the nitrite gel) (Fig. 4), makes the placement of the interface critical and explains the flux variations on a small scale (Table 3).

The NO_3^- increase in the water column in March in spite of its ingoing flux toward sediment seemed to be largely explained by allochthonous inputs. The influx in April and May could be in part explained by large nitrogen demand for denitrification in the upper layers of the sediment in winter. With regard to the degradation products of OM, the permanent ΣNH_3 outflows coincided with the progressive loading of the water column until April. The reverse of this trend in May despite the strong remobilization of ammonium at depth, and the not significant increase in SRP in the water column despite the SRP efflux in March and April could reflect a vegetation pumping of ammonium and P (explaining the downward shift of the P peak during this period, Fig. 3) or even primary producer bloom (Sand-Jensen and Borum, 1990; Rozan et al., 2002). Moreover, forms of water stratification which can exist in pounds or even marshes (Condie and Webster, 2001; Chimney et al., 2006) could counteract the link between fluxes at the interface and water column response, especially through the phosphate availability (Crockford et al., 2015). However, the shallow

depth of the marshes, the site's windward catch and the variations in water level caused by management of marsh water may favour the mixing and thus allow efficient nutrient accessibility throughout the water column.

However, this work strongly suggested the link between the outflow of SRP and the triggering of the nanophytoplankton development in April by reducing P limitation of this system, in addition to the physical parameters being favorable to such development. It highlighted the link between phytoplankton dynamics and mineralization processes by showing congruence between temporal patterns of benthic SRP regeneration and small phytoplanktonic cells (*i.e.* nano/picophytoplankton) development. Indeed, the evolution of N/P ratios strongly suggests a prevalence of internal recycling of P rather than external input for the development of phytoplankton. Although temporal patterns between benthic regeneration and planktonic production have potentially been shown in coastal environments (Kemp and Boyton, 1984; Cowan and Boyton, 1996), the high nitrate content at Marans influenced the dynamics of this system, both at the sediment compartment and the water column scale, which could decrease benthos-pelagos interactions (Kelly et al., 1985). Indeed, denitrification processes inhibited for about a month the respiration of metal oxides and thus the potential release of SRP into the water column. This phenomenon suggested a completely different behavior of the sediment compartment in lower nitrate systems, and therefore a different response of the chemical and biological parameters of the water column. However, the conceptual model presented in this work could be deployed in other sites of interest in order to propose new tools for observatories to characterize the aquatic environment quality and predict future trends.

5. Conclusions and perspectives

- The strong phosphate limitation and huge nitrogen content in water column suggested a high nitrate control on the temporal patterns of diagenetic processes and phytoplankton development.
- Denitrification processes inhibited phosphates mobilisation in winter by preventing iron hydroxide reduction and seemed to be the main route for nitrogen removal in the sediment.
- Depletion in nitrates in the sediment from early spring triggered iron hydroxide respiration and phosphate mobilisation on the upper part of the sediment. A significant phosphate efflux was observed in April, congruent with nanophytoplankton development.
- The multiscale heterogeneity on chemical species distribution highlighted the importance of biotic parameters on the distribution and mobilisation of such species in the sediment.
- The complexity in evaluating nutrient flux feedback on the water column leads to the necessity of a better understanding of the nutrient catchment control by autotrophs.
- An annual monitoring in such anthropogenic environment, duplicated on less nitrate-rich systems would provide a broader view of the importance and prediction of sediment-water column coupling in Charente Maritime freshwater marshes and temperate marshes in general.

Acknowledgments

This study was supported by the « Ministère de l'Enseignement Supérieur et de la Recherche », the water agencies Loire-Bretagne and Adour-Garonne, conseil général de Charente-Maritime, European Union. This research was supported by a PhD grant from CDA Agglomération of La Rochelle. We acknowledge the AutoAnalyzer plat-form for analysis of nutrients at LIENSs laboratory and ICPMS plat-form for metal analysis at Nantes. Thanks, are extended to the UNIMA (Union des Marais de Charente-Maritime), FMA and stakeholders for their expertise on the Charente-Maritime marshes.

REFERENCES

Aller, R. C. (2004). Conceptual models of early diagenetic processes: The muddy seafloor as an unsteady, batch reactor. Journal of Marine Research, 62, 815-835.

Aller, R.C., Aller, J.Y., Zhu, Q., Heilbrun, C., Klingensmith, I. and Kaushik, A. (2019). Worm tubes as conduits for the electrogenic microbial grid in marine sediments. Science Advance, 5, 1-8.

Anschutz, P., Hyacinthe, C., Carbonel, P., Jouanneau, J. M. and Jorissen, F. (1999). La distribution du phosphore inorganique dans les sédiments modernes du golfe de Gascogne. Earth and Planetary Sciences, 328, 765-771.

Anschutz, P., Zhong, S., Sundby, B., Mucci, A. and Gobeil, C. (1998). Burial efficiency of phosphorus and the geochemistry of iron in continental margin sedime. Limnology and Oceanography, 43, 53-64.

Barrow, J. L., Beisner, B. E., Giles, R., Giani, A., Domaizon, I. and Gregory-Eaves, I. (2019). Macrophytes moderate the taxonomic and functional composition of phytoplankton assemblages during a nutrient loading experiment. Freshwater Biology, 64, 1369-1381.

Berg, P., Risgaard-Petersen, N. and Rysgaard, S. (1998). Interpretation of measured concentration profiles in sediment pore water. Limnology and Oceanography, 43, 1500-1510.

Binnerup, S. J., Jensen, K., Revsbech, N. P., Jensen, M. H. and Sorensen, J. (1992). Denitrification, dissimilatory reduction of nitrate to ammonium, and nitrification in a bioturbated estuarine sediment as measured with 15 N and microsensor techniques. Applied and Environmental Microbiology, 58, 303-313.

Borggaard, O. K., Jorgensen, S. S., Moberg, J. P. and Raben- Lange, B. (1990). Influence of organic matter on phosphate adsorption by aluminium and iron oxides in sandy soils. Journal of Soil Science, 41, 443-449.

Boström, B., Andersen, J. M., Fleischer, S. and Jansson, M. (1988). Exchange of phosphorus across the sediment-water interface. Hydrobiologia, 170, 229-244.

Boudreau, B. P. (1997). Diagenetic models and their implementation. Springer, Berlin, 430p.

Burgin, A. J., Yang, W. H., Hamilton, S. K. and Silver, W. L. (2011). Beyond carbon and nitrogen: How the microbial energy economy couples elemental cycles in diverse ecosystems. Frontiers in Ecology and the Environment, 9, 44-52.

Canfield, D.E., Jørgensen, B.B., Fossing, H., Glud, R., Gundersen, J., Ramsing, N.B., Thamdrup, B., Hansen, J.W., Nielsen, L.P. and Hall, P.O.J. (1993). Pathways of organic carbon oxidation in three continental margin sediments. Marine Geology, 113, 27-40.

Caraco, N., Cole, J. and Likens, G. E. (1990). A comparison of phosphorus immobilization in sediments of freshwater and coastal marine systems. Biogeochemistry, 9, 277-290.

Cesbron, F., Metzger, E., Launeau, P., Deflandre, B., Delgard, M. L., Thibault De Chanvalon, A., Geslin, E., Anschutz, P. and Jézéquel, D. (2014). Simultaneous 2D imaging of dissolved iron and

reactive phosphorus in sediment porewaters by thin-film and hyperspectral methods. Environmental Science and Technology, 48, 2816-2826.

Chimney, M. J., Wenkert, L. and Pietro, K. C. (2006). Patterns of vertical stratification in a subtropical constructed wetland in south Florida (USA). Ecological Engineering, 27, 322-330.

Chmura, G. L., Anisfeld, S. C., Cahoon, D. R. and Lynch, J. C. (2003). Global carbon sequestration in tidal, saline wetland soils. Global Biogeochemical Cycles, 17, 1-12.

Christensen, K. K., Andersen, F. E. and Jensen, H. S. (1997). Comparison of iron, manganese, and phosphorus retention in freshwater littoral sediment with growth of Littorella uniflora and benthic microalgae. Biogeochemistry, 38, 149-171.

Cleveland, W. S. (1981). LOWESS: A program for smoothing scatterplots by robust locally weighted regression. The American Statistician, 35, 54.

Condie, S. A. and Webster, I. A. (2001). Estimating stratification in shallow water bodies from mean meteorological conditions. Journal of Hydraulic Engineering, 127, 288-292.

Cowan, J. L. W. and Boyton, W. R. (1996). Sediment-water oxygen and nutrient exchanges along the longitudinal axis of Chesapeake Bay: seasonal patterns, controlling factors and ecological significance. Estuaries, 19, 562-580.

Crockford, L., Jordan, P., Melland, A. R. and Taylor, D. (2015). Storm-triggered, increased supply of sediment-derived phosphorus to the epilimnion in a small freshwater lake. Inland Waters, 5, 15-26.

David, V., Tortajada, S., Philippine, O., Bréret, M., Barnett, A., Agogué, H., Robin, F. X. and Dupuy, C. (2020b). Ecological succession and resilience of plankton recovering from an acute disturbance in freshwater marshes. Science of the Total Environment, 709, 135997.

David, V., Tortajada, S., Savoye, N., Breret, M., Lachaussée, N., Philippine, O., Robin, F. X. and Dupuy, C. (2020a). Impact of human activities on the spatio-seasonal dynamics of plankton diversity in drained marshes and consequences on eutrophication. Water Research, 170.

Davison, W., Grime, G.W., Morgan, J.A.W. and Clarke, K. (1991). Distribution of dissolved iron in sediment pore waters at submillimetre resolution. Nature, 352, 323-325.

Ding, S., Chen, M., Gong, M., Fan, X., Qin, B., Xu, H., Gao, S., Jin, Z., Tsang, D. C. W. and Zhang, C. (2018). Internal phosphorus loading from sediments causes seasonal nitrogen limitation for harmful algal blooms. Science of the Total Environment, 625, 872-884.

Dupuy, C., Talarmin, A., Hartmann, H. J., Delmas, D., Courties, C. and Marquis, E. (2011). Community structure and grazing of the nano-microzooplankton on the continental shelf of the Bay of Biscay. Estuarine, Coastal and Shelf Science, 95, 1-13.

Ekholm, P. and Lehtoranta, J. (2012). Does control of soil erosion inhibit aquatic eutrophication? Journal of Environmental Management, 93, 140-146.

Frederiksen, M.S. and Glud, R.N. (2006). Oxygen dynamics in the rhizosphere of Zostera marina: A two-dimensional planar optode study. Limnology and Oceanography, 51, 1072-1083.

Froelich, P. N., Klinkhammer, G. P., Bender, M. L., Luedtke, N. A., Heath, G. R., Cullen, D., Dauphin, P., Hammond, D., Hartman, B. and Maynard, V. (1979). Early oxidation of organic matter in pelagic sediments of the eastern equatorial Atlantic: suboxic diagenesis. Geochimica et Cosmochimica Acta, 43, 1075-1090.

Gächter, R. and Müller, B. (2003). Why the phosphorus retention of lakes does not necessarily depend on the oxygen supply to their sediment surface. Limnology and Oceanography, 48, 929-933.

Giles, C. D., Isles, P. D. F., Manley, T., Xu, Y., Druschel, G. K. and Schroth, A. W. (2016). The mobility of phosphorus, iron, and manganese through the sediment–water continuum of a shallow eutrophic freshwater lake under stratified and mixed water-column conditions. Biogeochemistry, 127, 15-34.

Grenz, C., Moutin T., Picot, B. and Massé, H. (1991). Comparaison de deux méthodes de mesure de flux de nutriments à l'interface eau-sédiment : méthode des peepers et méthode des chambres

benthiques. Comptes rendus de l'Académie des sciences. Série III, Sciences de la vie, Elsevier, 313, 239-244.

Grüneberg, B., Dadi, T., Lindim, C. and Fischer, H. (2015). Effects of nitrogen and phosphorus load reduction on benthic phosphorus release in a riverine lake. Biogeochemistry, 123, 185-202.

Hansen, J., Reitzel, K., Jensen, H. S. and Andersen, F. (2003). Effects of aluminum, iron, oxygen and nitrate additions on phosphorus release from the sediment of a Danish softwater lake. Hydrobiologia, 492, 139-149.

Herzsprung, P., Schultze, M., Hupfer, M., Boehrer, B., Tümpling, W. v., Duffek, A., Duffek, A., Van der Veen, A. and Friese, K. (2010). Flood effects on phosphorus immobilisation in a river water filled pit lake-Case study Lake Goitsche (Germany). Limnologica, 40, 182-190.

Hlaili, A. S., Niquil, N. and Legendre, L. (2014). Planktonic food webs revisited: Reanalysis of results from the linear inverse approach. Progress in Oceanography, 120, 216-229.

Horppila, J. (2019). Sediment nutrients, ecological status and restoration of lakes. Water Research, 160, 206–208.

Hupfer, M. and Lewandowski, J. (2008). Oxygen controls the phosphorus release from lake sediments - A long-lasting paradigm in limnology. International Review of Hydrobiology, 93, 415-432.

Hyacinthe, C., Bonneville, S. and Van Cappellen, P. (2006). Reactive iron (III) in sediments: Chemical versus microbial extractions. Geochimica, 70, 4166-4180.

Jensen, H. S., Mortensen, P. B., Andersen, F. 0., Rasmussen, E. and Jensen, A. (1995). Phosphorus cycling in a coastal marine sediment, Aarhus Bay, Denmark. Limnology and Oceanography, 40, 908-917.

Jeppesen, E., Søndergaard, M., Jensen, J. P., Havens, K. E., Anneville, O., Carvalho, L., Covenay, M. F., Deneke, R., Dokulil, M. T., Foy, B., Gerdeaux, D., Hampton, S. E., Hilt, S., Kangur, K., Köler, J., Lammens, E. H. H. R., Lauridsen, T. L., Manca, M., Miracle, M. R., Moss, B., Noges, P., Persson, G., Phillips, G., Portielje, R., Romo, S., Schelske, C. L., Straile, D., Tatrai, I., Willen, E.

and Winder, M. (2005). Lake responses to reduced nutrient loading - An analysis of contemporary long-term data from 35 case studies. Freshwater Biology, 50, 1747-1771.

Jézéquel, D., Brayner, R., Metzger, E., Viollier, E., Prévot, F. and Fiévet, F. (2007). Two-dimensional determination of dissolved iron and sulfur species in marine sediment pore-waters by thin-film based imaging. Thau lagoon (France). Estuarine, Coastal and Shelf Science, 72, 420-431.

Johnston, S. G., Burton, E. D., Aaso, T. and Tuckerman, G. (2014). Sulfur, iron and carbon cycling following hydrological restoration of acidic freshwater wetlands. Chemical Geology, 371, 9-26.

Justić, D., Rabalais, N. N., Turner, R. E. and Dortch, Q. (1995). Changes in nutrient structure of river-dominated coastal waters: Stoichiometric nutrient balance and its consequences. Estuarine, Coastal and Shelf Science, 40, 339-356.

Kelly, J., Berounsky, V., Nixon, S. and Oviatt, C. (1985). Benthic-pelagic coupling and nutrient cycling across an experimental eutrophication gradient. Marine Ecology Progress Series, 26, 207-219.

Kemp, W. M. and Boynton, W. R. (1984). Spatial and temporal coupling of nutrient inputs to estuarine primary production: the role of particulate transport and decomposition. Bulletin of Marine Science, 35, 522-535.

Kostka, J. E. and Luther, G. W. (1993). Partitioning and speciation of solid phase iron in saltmarsh sediments. Geochimica et Cosmochimica Acta, 58, 1701-1710.

Kraal, P., Burton, E. D., Rose, A. L., Kocar, B. D., Lockhart, R. S., Grice, K., Bush, R. T., Tan, E. and Webb, S. M. (2015). Sedimentary iron-phosphorus cycling under contrasting redox conditions in a eutrophic estuary. Chemical Geology, 392, 19-31.

Legendre, L. and Rassoulzadegan, F. (1995). Plankton and nutrient dynamics in marine waters. Ophelia, 41, 153-172.

Lehtoranta, J. and Heiskanen, A. (2003). Dissolved iron: phosphate ratio as an indicator of phosphate release to oxic water of the inner and outer coastal Baltic Sea. Hydrobiologia, 492, 69-84.

Lewandowski, J., Rüter, K. and Hupfer, M. (2002). Two-dimensional small-scale variability of pore water phosphate in freshwater lakes: Results from a novel dialysis sampler. Environmental Science and Technology, 36, 2039-2047.

Li, Y. H. and Gregory, S. (1974). Diffusion of ions in sea water and in deep-sea sediments. Geochimica et Cosmochimica Acta, 38, 703-714.

Liu, J., Luo, X., Zhang, N., Wu, Y. (2016). Phosphorus released from sediment of Dianchi Lake and its effect on growth of *Microcystis aeruginosa*. Environmental Science and Pollution Research, 23, 16321-16328.

Lynn, D. H. (2003). The journal of eukaryotic microbiology. Journal of Eukaryotic Microbiology, 50, 1-2.

Masclaux, H., Tortajada, S., Philippine, O., Robin, F. X. and Dupuy, C. (2014). Planktonic food web structure and dynamic in freshwater marshes after a lock closing in early spring. Aquatic Sciences, 77, 115-128.

Metzger, E., Thibault De Chanvalon, A., Cesbron, F., Barbe, A., Launeau, P., Jézéquel, D. and Mouret, A. (2016). Simultaneous Nitrite/Nitrate Imagery at Millimeter Scale through the Water-Sediment Interface. Environmental Science and Technology, 50, 8188-8195.

Middelburg, J.J., Soetaert, K., Herman, P.M.J. and Heip, C.H.R. (1996). Denitrification in marine sediments: A model study. Global Biogeochemical Cycles, 10, 661-673.

Millero, F. J., Sotolongo, S. and Izaguirre, M. (1987). Oxidation kinetics of Fe (II) in sea water. Geochimica et Cosmochimica Acta, 51, 793-801.

Morais, P., Chícharo, M. A. and Barbosa, A. (2003). Phytoplankton dynamics in a coastal saline lake (SE-Portugal). Acta Oecologica, 24, 87-96.

Neupane, G., Donahoe, R. J. and Arai, Y. (2014). Kinetics of competitive adsorption/desorption of arsenate and phosphate at the ferrihydrite-water interface. Chemical Geology, 368, 31-38.

Pagès, A., Teasdale, P.R., Robertson, D., Bennett, W.W., Schäfer, J. and Welsh, D.T. (2011). Representative measurement of two-dimensional reactive phosphate distributions and co-distributed iron(II) and sulfide in seagrass sediment porewaters. Chemosphere, 85, 1256-1261.

Pan, F., Guo, Z., Cai, Y., Fu, Y., Wu, J., Wang, B., Liu, H. and Gao, A. (2020). Cyclical patterns and (im)mobilization mechanisms of phosphorus in sediments from a small creek estuary: Evidence from *in situ* monthly sampling and indoor experiments. Water Research, 171, 115479.

Pan, F., Liu, H., Guo, Z., Li, Z., Wang, B., Cai, Y. and Gao, A. (2019). Effects of tide and season changes on the iron-sulfur-phosphorus biogeochemistry in sediment porewater of a mangrove coast. Journal of Hydrology, 568, 686-702.

Pastor, L., Rabouille, C., Metzger, E., Thibault de Chanvalon, A., Viollier, E. and Deflandre, B. (2018). Transient early diagenetic processes in Rhône prodelta sediments revealed in contrasting flood events. Continental Shelf Research, 166, 65-76.

Perkins, R. G. and Underwood, G. J. C. (2001). The potential for phosphorus release across the sediment-water interface in an eutrophic reservoir dosed with ferric sulphate. Water Research, 35, 1399-1406.

Petzoldt, T. and Uhlmann, D. (2006). Nitrogen emissions into freshwater ecosystems: Is there a need for nitrate elimination in all wastewater treatment plants? Acta Hydrochimica et Hydrobiologica, 34, 305-324.

Rasmussen, H. and Jorgensen, B.B. (1992). Microelectrode studies of seasonal oxygen uptake in a coastal sediment: role of molecular diffusion. Marine Ecology Progress Series, 81, 289-303.

Rebreanu, L., Vanderborght, J. P. and Chou, L. (2008). The diffusion coefficient of dissolved silica revisited. Marine Chemistry, 112, 230-233.

Redfield, A. C. (1958). The biological control of chemical factors in the environment. American Scientist, 46, 205-221.

Reid, P. C., Lancelot, C., Gieskes, W. W. C., Hagmeier, E. and Weichart, G. (1990). Phytoplankton of the North Sea and its dynamics: A review. Netherlands Journal of Sea Research, 26, 295-331.

Revsbech, N.P. (1989). An oxygen microsensor with a guard cathode. Limnology and Oceanography, 34, 474-478.

Rozan, T. F., Taillefert, M., Trouwborst, R. E., Glazer, B. T., Ma, S., Herszage, J., Valdes, L. M., Price, K. S. and Luther, G. W. (2002). Iron-sulfur-phosphorus cycling in the sediments of a shallow coastal bay: Implications for sediment nutrient release and benthic macroalgal blooms. Limnology and Oceanography, 47, 1346-1354.

Rysgaard, S., Risgaard-Petersen, N., Nielsen, L. P. and Revsbech, N. P. (1993). Nitrification and denitrification in lake and estuarine sediments measured by the 15N dilution technique and isotope pairing. Applied and Environmental Microbiology, 59, 2093-2098.

Sand-Jensen, K. and Borum, J. (1991). Interactions among phytoplankton, periphyton, and macrophytes in temperate freshwaters and estuaries. Aquatic Botany, 41, 137-175.

Santner, J., Larsen, M., Kreuzeder, A. and Glud, R.N. (2015). Two decades of chemical imaging of solutes in sediments and soils - a review. Analytica Chimica Acta, 878, 9-42.

Sarazin, G., Michard, G. and Prevot, F. (1999). A rapid and accurate spectroscopic method for alkalinity measurements in sea water samples. Water Research, 33, 290-294.

Schauser, I., Chorus, I. and Lewandowski, J. (2006). Effects of nitrate on phosphorus release: Comparison of two Berlin lakes. Acta Hydrochimica et Hydrobiologica, 34, 325-332.

Schindler, D. W. (1974). Eutrophication and recovery in experimental lakes: Implications for lake management. Science, 184, 897-899.

Sholkovitz, E. (1973). Interstitial water chemistry of the Santa Barbara Basin sediments. Geochimica et Cosmochimica Acta, 37, 2043-2073.

Smith, R.L., Böhlke, J.K., Song, B. and Tobias, C.R. (2015). Role of Anaerobic Ammonium Oxidation (Anammox) in Nitrogen Removal from a Freshwater Aquifer. Environmental Science and Technology, 49, 12169-12177.

Smith, V. H. (2003). Eutrophication of freshwater and coastal marine ecosystems a global problem. Environmental Science and Pollution Research, 10, 126-139.

Smolders, E., Baetens, E., Verbeeck, M., Nawara, S., Diels, J., Verdievel, M., Peeters, B., De Cooman, W. and Baken, S. (2017). Internal Loading and Redox Cycling of Sediment Iron Explain Reactive Phosphorus Concentrations in Lowland Rivers. Environmental Science and Technology, 51, 2584-2592.

Soballe, D. M. and Kimmel, B. L. (1987). A large-scale comparison of factors influencing phytoplankton abundance in rivers, lakes, and impoundments. Ecology, 68, 1943-1954.

Søndergaard, M., Lauridsen, T. L., Johansson, L. S. and Jeppesen, E. (2017). Nitrogen or phosphorus limitation in lakes and its impact on phytoplankton biomass and submerged macrophyte cover. Hydrobiologia, 795, 35-48.

Søndergaard , M., Jeppesen, E., and Jensen, J. P. (2000). Hypolimnetic Nitrate Treatment to Reduce Internal Phosphorus Loading in a Stratified Lake. Lake and Reservoir Management, 16, 195-204.

Sousa, A. I., Lillebø, A. I., Pardal, M. A. and Caçador, I. (2010). Productivity and nutrient cycling in salt marshes: Contribution to ecosystem health. Estuarine, Coastal and Shelf Science, 87, 640-646.

Thibault de Chanvalon, A., Metzger, E., Mouret, A., Knoery, J., Geslin, E. and Meysman, F. J. R. (2017). Two dimensional mapping of iron release in marine sediments at submillimetre scale. Marine Chemistry, 191, 34-49.

Thibault de Chanvalon, A., Mouret, A., Knoery, J., Geslin, E., Péron, O. and Metzger, E. (2016). Manganese, iron and phosphorus cycling in an estuarine mudflat, Loire, France. Journal of Sea Research, 118, 92-102.

Thyssen, M., Mathieu, D., Garcia, N. and Denis, M. (2008). Short-term variation of phytoplankton assemblages in Mediterranean coastal waters recorded with an automated submerged flow cytometer. Journal of plankton research, 30, 1027-1040.

Toompuu, A., Carstensen, J. and Müller-Karulis, B. (2003). Seasonal variation of average phytoplankton concentration in the Kattegat - A periodical point model. Journal of Sea Research, 49, 323-335.

Tortajada, S., David, V., Brahmia, A., Dupuy, C., Laniesse, T., Parinet, B., Pouget, F., Rousseau, F., Simon-Bouhet, B. and Robin, F. X. (2011). Variability of fresh- and salt-water marshes characteristics on the west coast of France: A spatio-temporal assessment. Water Research, 45, 4152-4168.

Van Dael, T., De Cooman, T., Verbeeck, M. and Smolders, E. (2020). Sediment respiration contributes to phosphate release in lowland surface waters. Water Research, 168, 115168.

Viollier, E., Rabouille, C., Apitz, S.E., Breuer, E., Chaillou, G., Dedieu, K., Furukawa, Y., Grenz, C., Hall, P., Janssen, F., Morford, J.L., Poggiale, J.C., Roberts, S., Shimmield, T., Taillefert, M., Tengberg, A., Wenzhöfer F. and Witte, U. (2003). Benthic biogeochemistry: State of the art technologies and guidelines for the future of in situ survey. Journal of Experimantal Marine Biology and Ecology, 285-286, 5-31.

Wauer, G., Gonsiorczyk, T., Casper, P. and Koschel, R. (2005). P-immobilisation and phosphatase activities in lake sediment following treatment with nitrate and iron. Limnologica, 35, 102-108.

Welch, E. B. and Cooke, G. D. (2005). Internal phosphorus loading in shallow lakes: Importance and control. Lake and Reservoir Management, 21, 209-217.

Withers, P. J. A. and Jarvie, H. P. (2008). Delivery and cycling of phosphorus in rivers: A review. Science of the Total Environment, 400, 379-395.

Wu, Z., Liu, Y., Liang, Z., Wu, S. and Guo, H. (2017). Internal cycling, not external loading, decides the nutrient limitation in eutrophic lake: A dynamic model with temporal Bayesian hierarchical inference. Water Research, 116, 231-240.

Xiao, Y., Cheng, H., Zhu, X. and Tang, H. (2015). Experimental study on adsorption of phosphorus on sediment components with different particle sizes. Environmental Engineering and Management Journal, 14, 2493-2500.

Yentsch, C. S. and Menzel, D. W. (1963). A method for the determination of phytoplankton chlorophyll and phaeophytin by fluorescence. Deep-Sea Research, 10, 221-231.

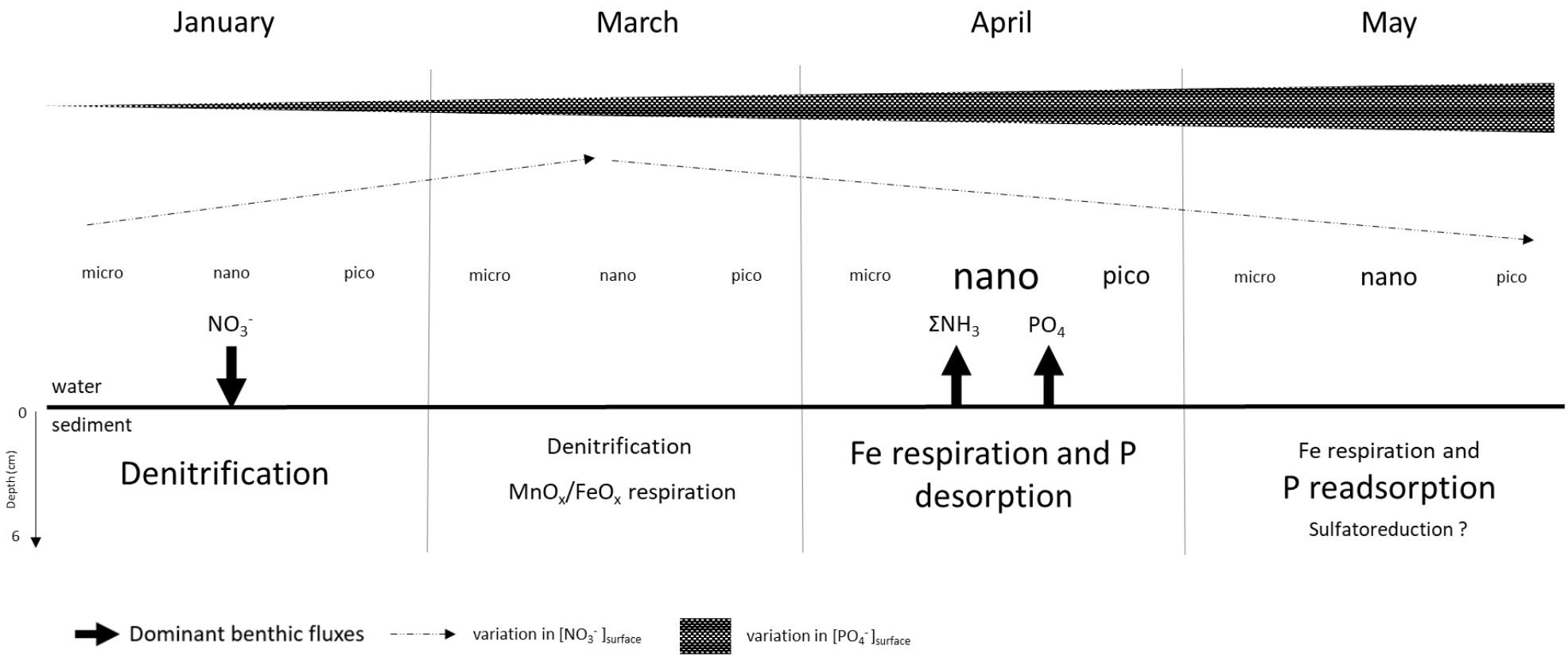
January
March
April
May
micro
nano
pico
micro
nano
pico
micro
nano
pico
micro
nano
pico
NO_3^-
ΣNH_3
PO_4
water
sediment
0
6
Depth (cm)
Denitrification
Denitrification
MnO_x/FeO_x respiration
Fe respiration and P desorption
Fe respiration and
P readsorption
Sulfatoreduction ?
Dominant benthic fluxes
variation in $[NO_3^-]_{surface}$
variation in $[PO_4^-]_{surface}$

Graphical abstract. Monthly *in situ* monitoring of the coupling between the sedimentary compartment and the water column in a temperate freshwater marsh.

Font: Times New Roman, 12. No color required.

Concentrations (µmol L^{-1})	NO_3^-	NO_2^-	$\sum NH_3$	SRP	Si
January	368.61	7.84	17.46	0.10	100.57
March	667.89 ± 66.44	4.93 ± 1.19	21.50 ± 2.49	BQL	70.29 ± 10.90
April	401.97 ± 6.60	20.43 ± 0.77	78.63 ± 0.40	0.14 ± 0.14	154.26 ± 17.89
May	370.78 ± 81.03	11.74 ± 3.30	70.14 ± 28.95	0.37 ± 0.02	124.33 ± 34.50

Table 1
Average nutrient concentrations (mean ± sd) in core bottom water in January, March, April and May 2019 at Marans.

Font: Times New Roman, 12.

No color required.

Flux (nmol cm^{-2} s^{-1})	O_2	NO_3^-	NO_2^-	$\sum NH_3$	SRP	Si	Fe^{2+}
January	1.67E-02 ± 1.45E-03	4.53E-03 ± 1.47E-03	5.06E-04 ± 1.71E-04	-1.30E-05 ± 6.11E-05	1.31E-06 ± 8.23E-07	-2.00E-04 ± 1.17E-04	-2.10E-06 ± 3.68E-06
March	1.46E-02 ± 1.28E-03	7.59E-04 ± 7.71E-04	1.01E-04 ± 1.01E-04	-1.16E-04 ± 8.04E-05	-1.00E-05 ± 7.06E-06	-5.65E-04 ± 2.59E-04	-1.85E-04 ± 9.43E-05
April	2.04E-02 ± 2.17E-03	9.19E-05 ± 7.01E-05	BQL	-1.04E-03 ± 9.76E-05	-1.10E-04 ± 2.81E-05	-4.82E-04 ± 2.46E-04	-1.97E-04 ± 5.02E-05
May	3.10E-02 ± 5.76E-03	1.56E-04 ± 1.14E-04	1.23E-06 ± 8.41E-07	-2.94E-04 ± 7.00E-04	-7.00E-06 ± 7.24E-06	-1.01E-03 ± 2.82E-04	-1.34E-04 ± 5.80E-05

Table 2

O_2, average nutrient and iron (Fe^{2+}) sediment-water interface fluxes (mean ± sd) at Marans in January, March, April and May 2019. For O_2, values corresponded to averages of 10 fluxes estimated on one core per date. For nutrients and Fe^{2+}, values correspond to averages of 3 fluxes estimated on each individual core. BQL corresponded to values below quantification limit.

Font: Times New Roman, 12.

No color required.

Species	Gel interface positioning	width-integrated average fluxes (nmol cm^{-2} s^{-1})		
		interface (mm)		
		-0.1	0	0.1
NO_2	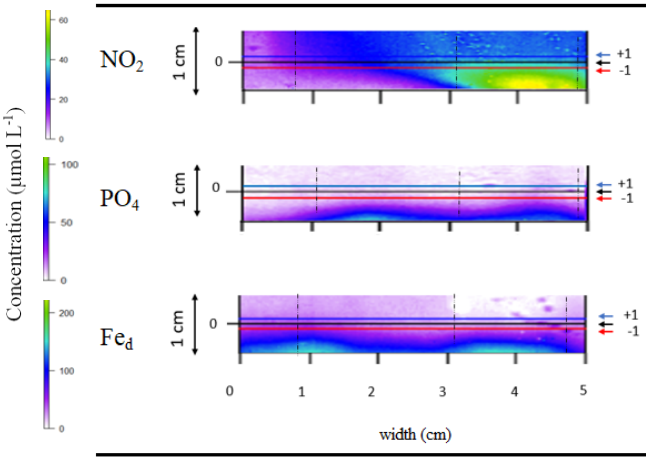	-5.69E-05	3.28E-05	1.12E-04
PO_4		-4.72E-05	3.85E-06	-6.82E-05
Fe_d		-4.23E-04	-2.49E-04	-5.25E-04

Table 3

Integrated average NO_2^- (probe 1), SRP and Fe_d (probe 2) fluxes at the 2D-gel interface as a function of the interface positioning (-1; 0; +1 mm).

Font: Times New Roman, 12.

Color required online only

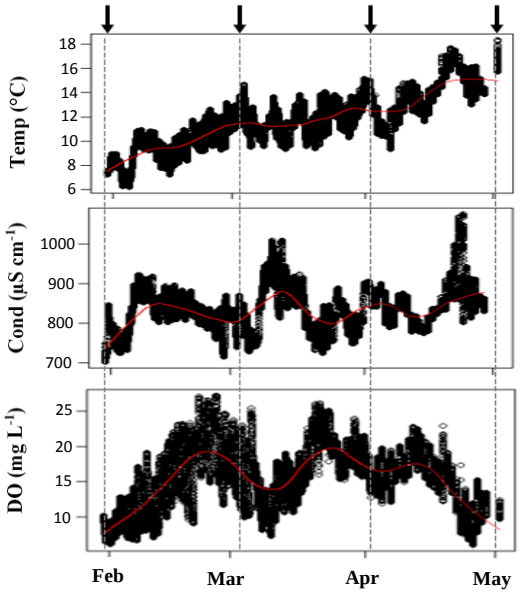

Fig. 1. Water column temperature (Temp), conductivity (Cond) and dissolved oxygen (DO) of Marans monitored continuously from January to May. Black arrows corresponded to the field campaigns. The red lines represented the LOWESS smoother of the data (Clevelend, 1981).

Font: Times New Roman, 12.

Color required online only.

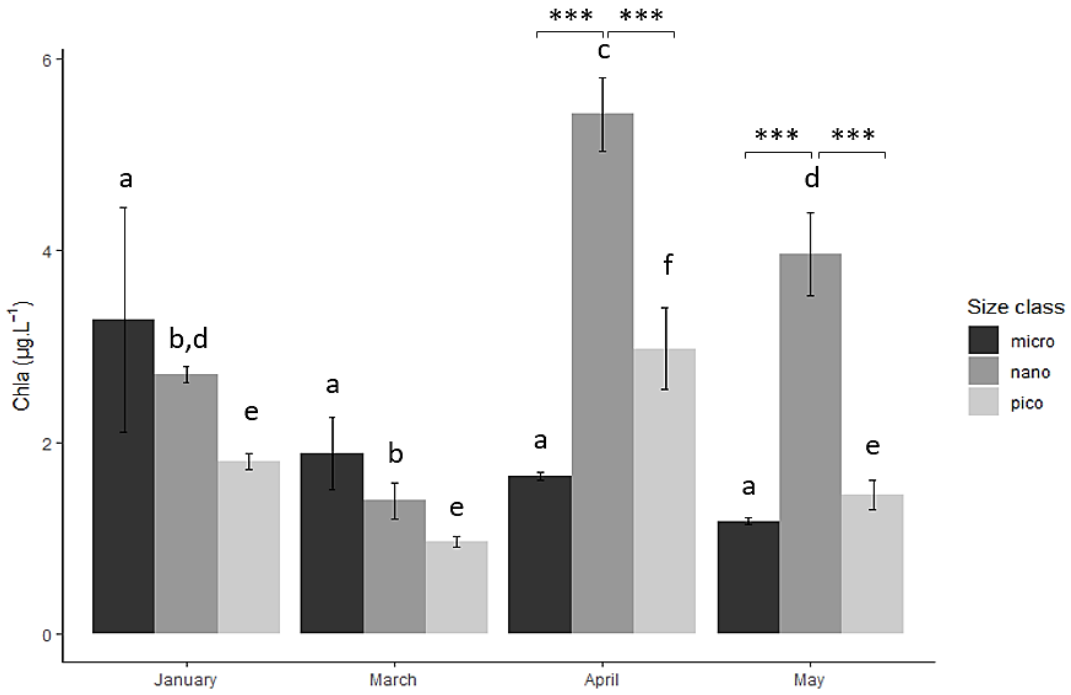

Fig. 2. Barplot showing the average chlorophyll *a* (Chla) biomasses (mean ± sd) by size class (micro: microphytoplankton (> 20 µm), nano: nanophytoplankton (3-20 µm), pico: picophytoplankton (< 3 µm)) at Marans in January, March, April and May 2019. The letters highlighted the significant differences between the dates at fixed size class. The stars highlighted the significant differences between the size classes at fixed date (ANOVA and Tuckey *post Hoc* tests, $\alpha<0.05$, $p<0.001$: ***).

Font: Times New Roman, 12.

Color required online only.

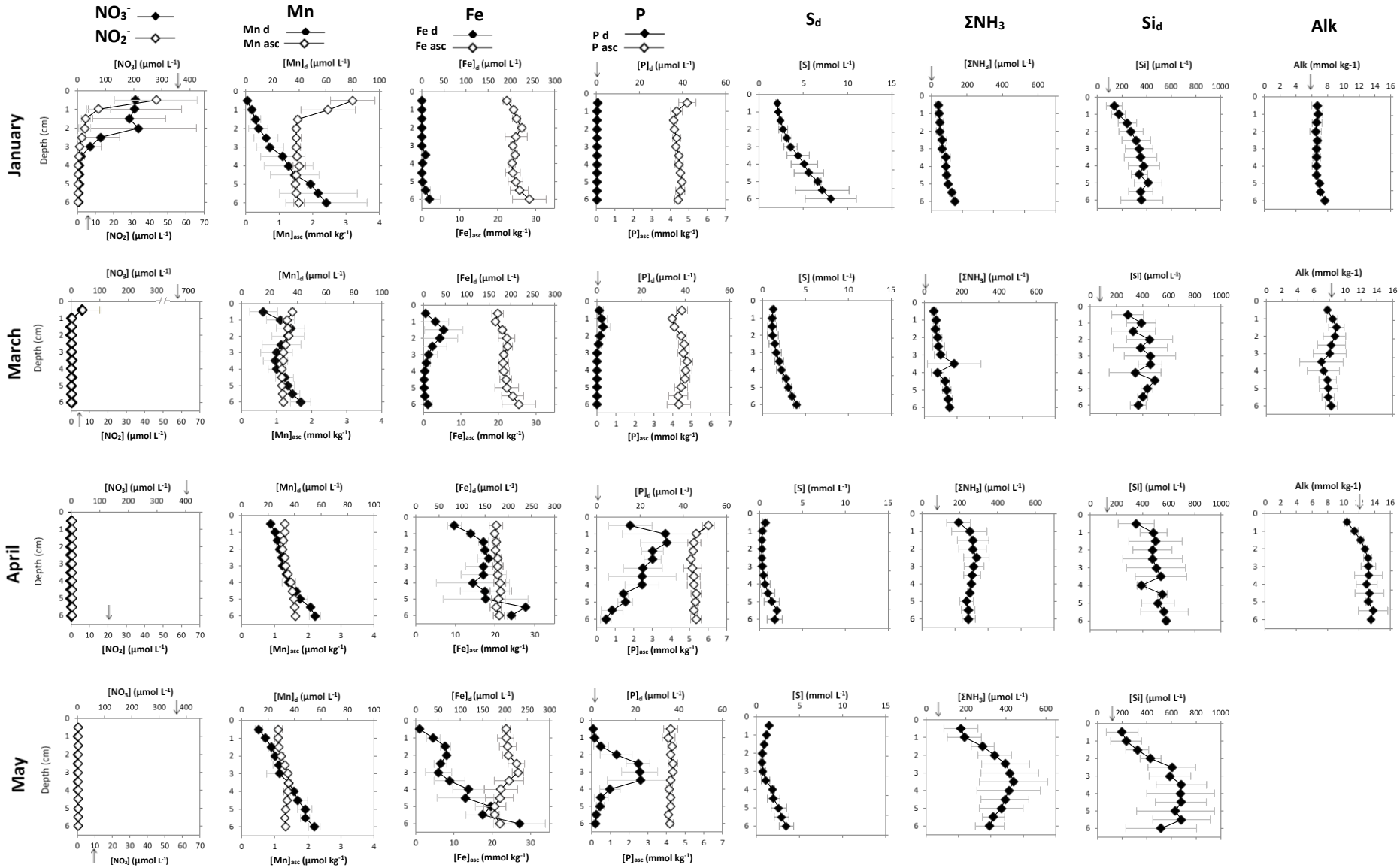
NO3-
NO2-
Mn
Mn d
Mn asc
Fe
Fe d
Fe asc
P
P d
P asc
Sd
ΣNH3
Sid
Alk
January
March
April
May
Depth (cm)
[NO3] (µmol L-1)
[NO2] (µmol L-1)
[Mn]d (µmol L-1)
[Mn]asc (mmol kg-1)
[Fe]d (µmol L-1)
[Fe]asc (mmol kg-1)
[P]d (µmol L-1)
[P]asc (mmol kg-1)
[S] (mmol L-1)
[ΣNH3] (µmol L-1)
[Si] (µmol L-1)
Alk (mmol kg-1)

Fig. 3. Dissolved NO_3^-, NO_2^-, Mn_d-Mn_{asc}, Fe_d-Fe_{asc}, SRP (P_d)-P_{asc}, SO_4 (S_d), ΣNH_3, Si_d, and alkalinity (Alk) profiles (mean ± sd) along the sediment column from 0 to 6 cm depth at Marans in January, March, April and May 2019. No data for alkalinity in May. The representation of standard deviation (n=3) indicates the spatial variability in the sediment. The arrows represented the concentration of the element under consideration in the water column.

Font: Times New Roman, 12.

Color required online only.

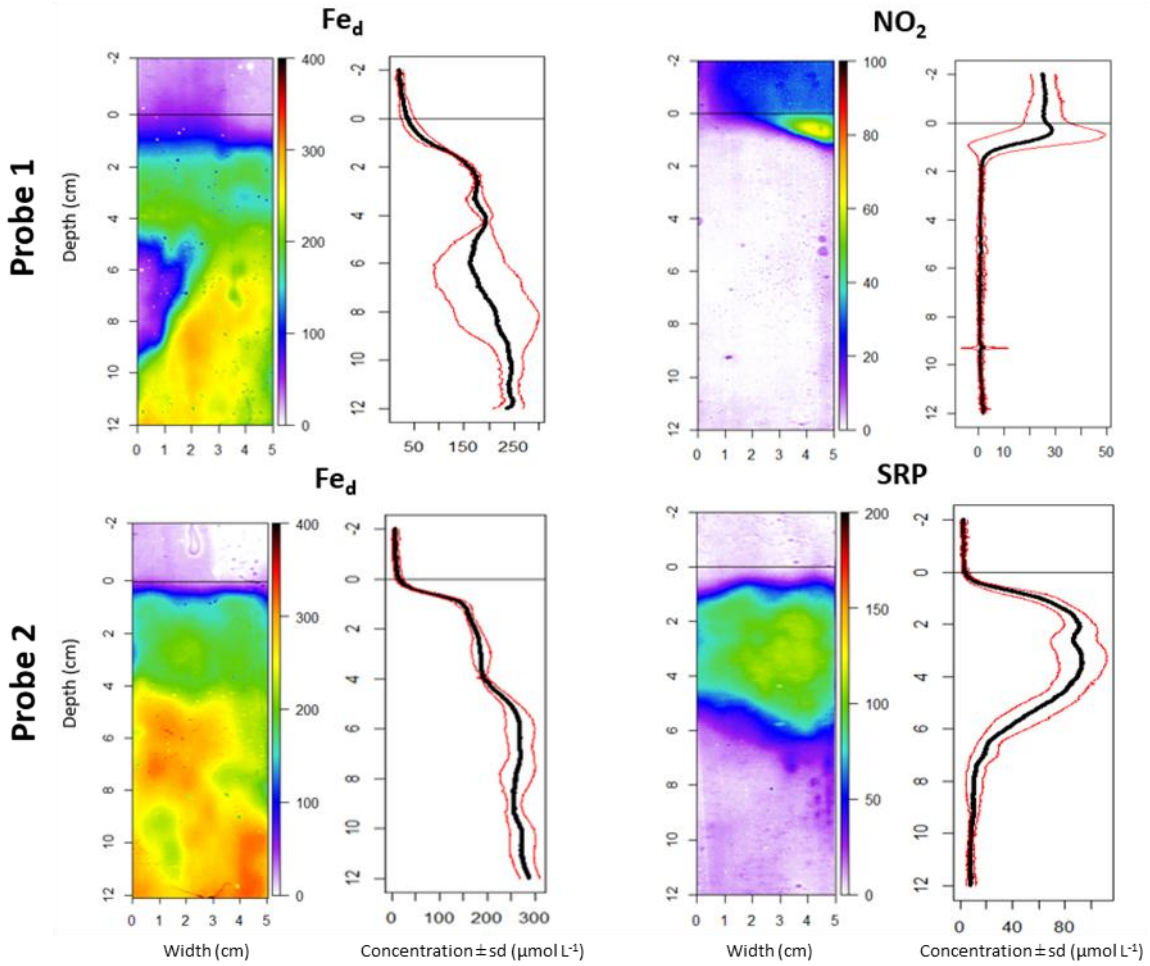

Fig. 4. 2D pore water distribution of iron (Fe_d) (probe 1 and 2), nitrite (NO_2) (probe 1) and soluble reactive phosphorus (SRP) (probe 2) concentrations of cores at Marans in April, and their associated 1D profile (black bold line represented the mean concentration, red lines, standard deviation). The horizontal black line represented the SWI. The color scale on the right of each image represented the concentrations in µmol L^{-1}. The probes came from two different cores.

Font: Times New Roman, 12.

Color required online only.

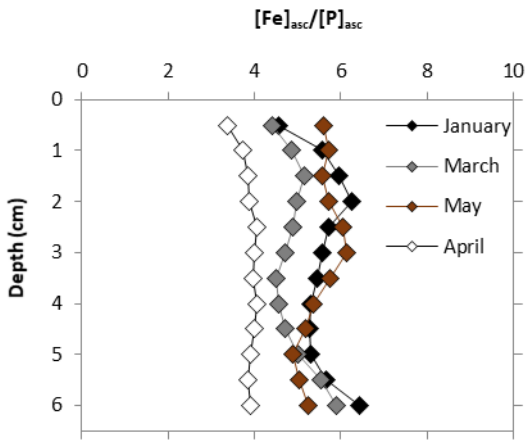

Fig. 5. $[Fe]_{asc}/[P_{asc}]$ ratio along the sediment column from 0 to 6 cm at Marans in January, March, April and May 2019.

Font: Times New Roman, 12.

Color required online only.

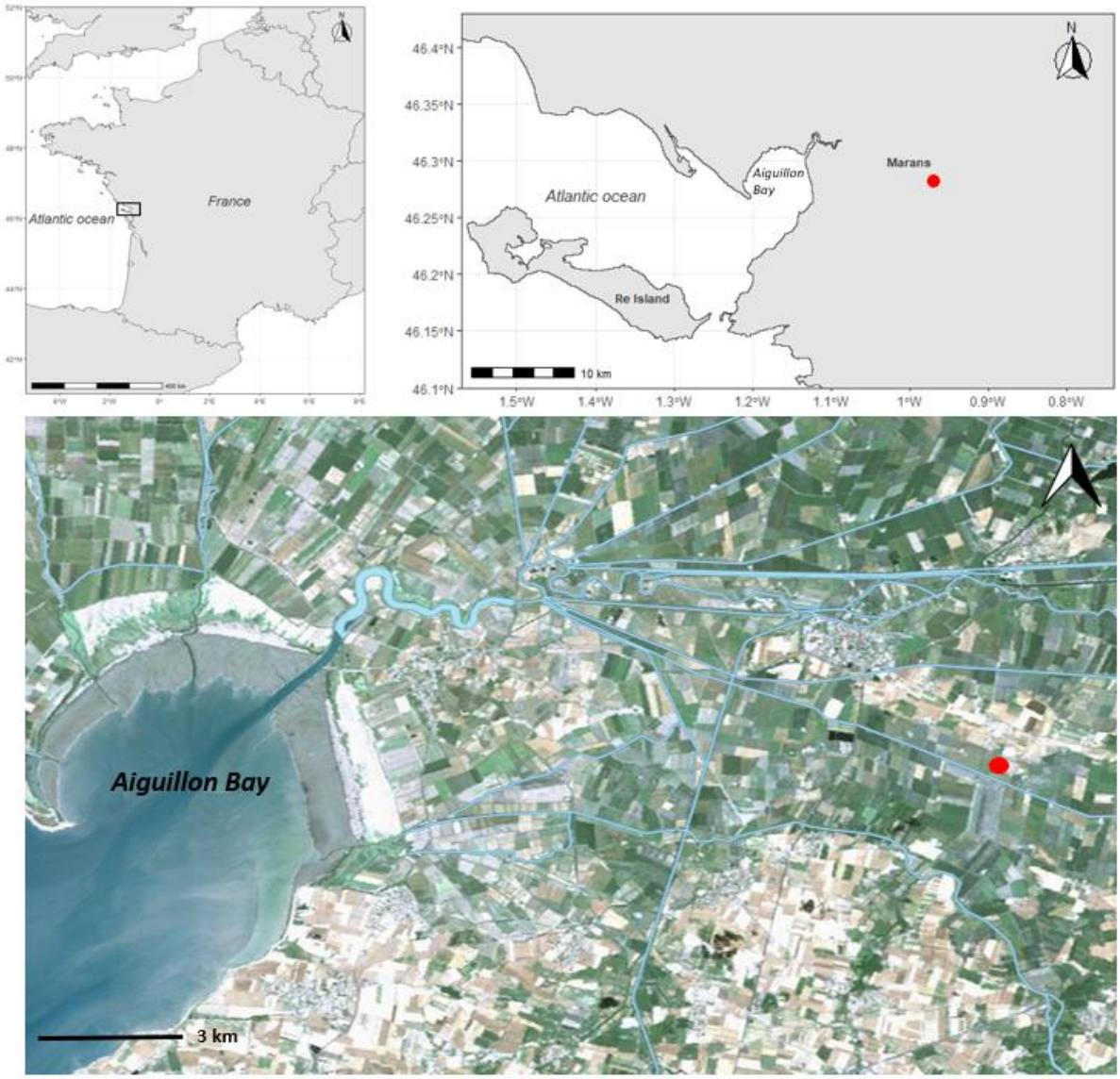

Fig. S1. Study region and sampling site (red point). The satellite image highlights the presence of crops around the study site (Google Earth). Blue lines represent the principal hydrographic network.

Font: Times New Roman, 12.

Color required.

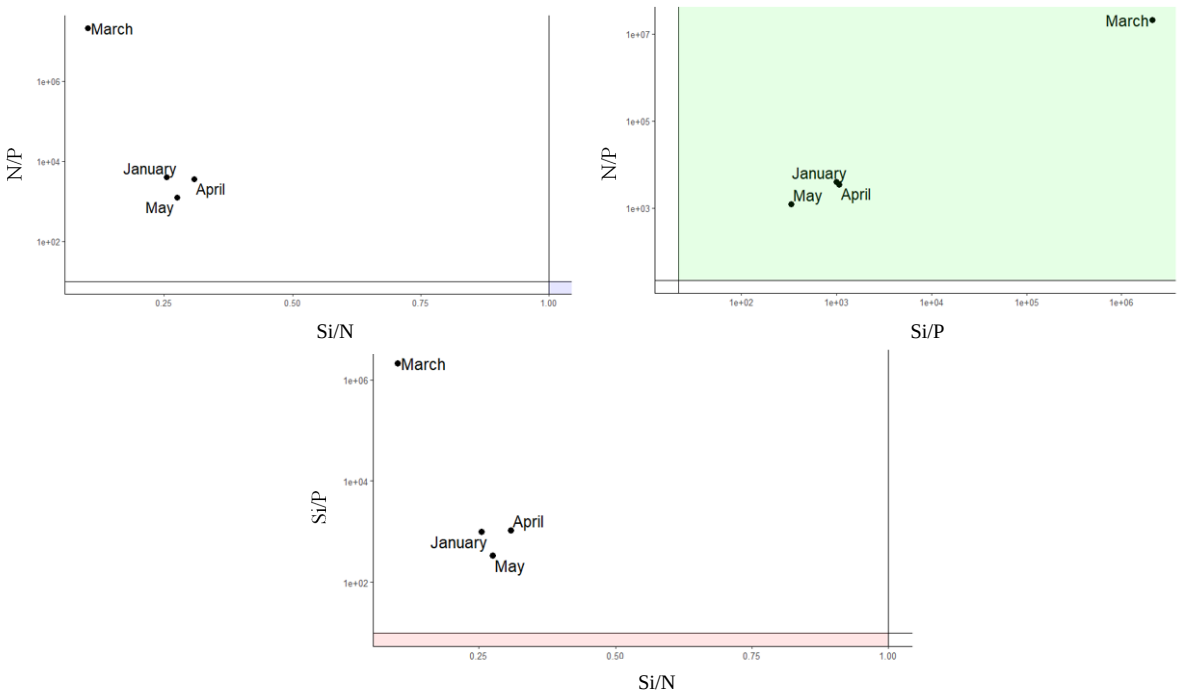

Fig. S2. Potential nutrient limitation following the Redfield ratios for Marans in January, March, April and May 2019. The black lines represent the limitation thresholds of ratio pairs. The stations in the colored zones are N-limited (blue), P-limited (green) and Si-limited (pink).

Font: Times New Roman, 12.

Color required online only.